High-pressure Phase Transition and Properties of Cu_3N: An Experimental and Theoretical Study

Aron Wosylus,[a] Ulrich Schwarz,[a] Lev Akselrud,[a] Matt G. Tucker,[b] Michael Hanfland,[c] Kaneez Rabia,[d] Christine Kuntscher,[d] Jörg von Appen,[e] Richard Dronskowski,[e] Dieter Rau,[f] and Rainer Niewa*[f]

Dedicated to Professor Martin Jansen on the Occasion of His 65th Birthday

Keywords: High-pressure chemistry; Copper; Nitrides; Phase transitions; Electronic structure calculations

Abstract. In-situ X-ray and neutron diffraction investigations on Cu_3N indicate the onset of a high-pressure phase transition at about 5 GPa. The tetragonal cell parameters of the high-pressure phase reveal a discontinuous volume decrease of about 20 %. The phase transition is reversible, with a hysteresis of about 2 GPa. Subsequent ex-situ investigations in a multi-anvil press evidence a reversible re-formation of ambient pressure Cu_3N from XRD patterns. The structure refinement with nitrogen atoms disordered in distorted octahedral voids of a tetragonal body-centered copper substructure leads to an occupation of approximately $^1/_3$ and thus to a composition of $Cu_3N_{1.0(1)}$. Optical absorption measurements (IR-VIS) up to 10 GPa indicate a semiconductor–metal transition. Density-functional based total energy calculations concerning the proposed high-pressure phase of Cu_3N strongly support the experimental findings of a pressure-induced phase transition above 6 GPa to a structure with a copper tetragonal body-centered sublattice and nitrogen atoms in distorted octahedral voids. However, the calculations identify a need for an ordered alternative to provide the tetragonal distortion within the range of the observed *c*/*a* ratio. The resulting lattice parameters and the transition pressure fit with the measured data. For the case of an ordered occupation of the copper *bct* octahedral voids, all observed properties are in good agreement with the calculations.

Introduction

The semiconducting nitride Cu_3N was first synthesized by *Juza* and *Hahn* in 1938 and is since known to crystallize in a so-called inverse ReO_3 crystal structure (Figure 1), an exclusive situation for binary transition metal nitrides [1, 2]. Because of its low density, which is due to large open voids, this type of atomic arrangement qualifies as a likely candidate for pressure-induced phase transitions. This assumption is also supported by the experimental observation of a structural change of the parent compound ReO_3 upon compression [3]. Moreover, the results of electronic structure calculations [4, 5] indicate a pressure-induced phase transition of ReO_3-type Cu_3N between 15 GPa and 35 GPa probably subsequent to a semiconductor-metal transition. A very detailed work of *Jan-*

* Prof. Dr. R. Niewa
Fax: +49-711-685-64241
E-Mail: rainer.niewa@iac.uni-stuttgart.de
[a] Max-Planck-Institut für Chemische Physik fester Stoffe
Nöthnitzer Straße 40
01187 Dresden, Germany
[b] Rutherford Appleton Laboratory
ISIS Facility
Didcot OX11
0Qx, Oxon, UK
[c] European Synchrotron Radiation Facility
38043 Grenoble, France
[d] Lehrstuhl für Experimentalphysik II
Institut für Physik
Universität Augsburg
Universitätsstraße 1
86159 Augsburg, Germany
[e] Institute of Inorganic Chemistry
RWTH Aachen University
Landoltweg 1
52074 Aachen, Germany
[f] Institut für Anorganische Chemie
Universität Stuttgart
Pfaffenwaldring 55
70569 Stuttgart, Germany

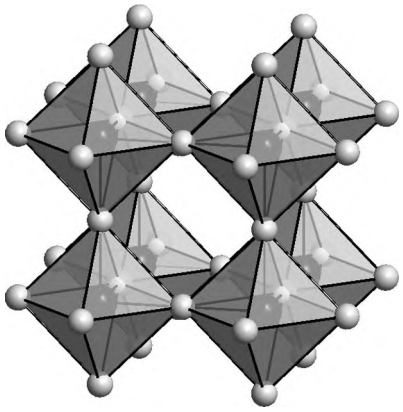

Figure 1. Crystal structure of the low-pressure modification of Cu_3N (ReO_3 type). White spheres correspond to copper atoms, the vertex-sharing coordination octahedra surrounding nitrogen are indicated.

sen et al. [4] recently investigated many promising high-pressure structure candidates by means of electronic structure calculations. The most promising has been identified to be the Li_3P structure type, the K_3N type, and the UO_3 type with transition pressures between 25 and 35 GPa. Contrary to this work, a second theoretical contribution [5] suggested the Cu_3Au structure type for HP-Cu_3N with a transition pressure of 17 GPa. However, so far reliable experimental high-pressure structure data are not available. Recently, independent from the investigations presented here, the electrical resistivity of Cu_3N was studied in dependence of pressure, resulting in a likely metallization above about 5 GPa [6, 7].

Results and Discussion

In a first series of experiments, Cu_3N was treated at high pressures and high temperatures up to p = 9 GPa and T = 500(80) K in a Walker type module before temperature quenching and pressure release. Analyses of the experiments reveal that the transformation products depend critically on the experimental conditions: We observed either the normal pressure modification of copper nitride (LP-Cu_3N) or copper metal intermixed with copper nitride. The recovered ambient pressure modification of Cu_3N exhibits a significantly increased full width at half maximum of the diffraction lines, which is in accordance with a reversible phase transition. Figure 2 shows a comparison of diffraction patterns of LP-Cu_3N before and after a pressure experiment. The formation of copper metal in some experiments is attributed to pressure gradients and shear stresses in the octahedra and the metastable nature of Cu_3N.

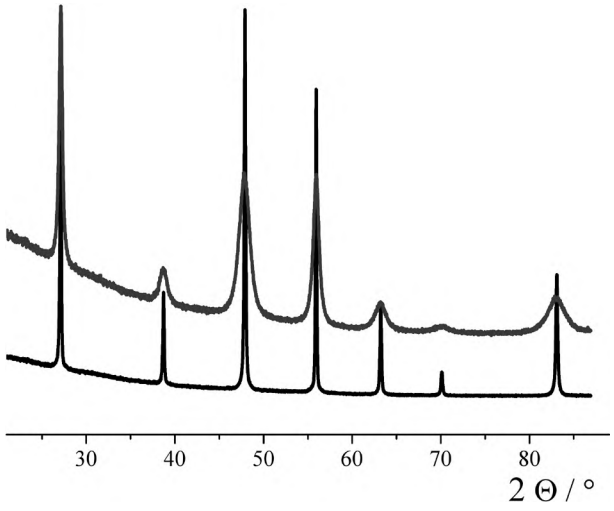

Figure 2. XRD pattern of LP-Cu_3N before (bottom line) and after (top line) a pressure treatment in the multi-anvil cell at about 9 GPa (Co-$K_{\alpha 1}$ radiation).

In-situ X-ray diffraction investigations, carried out in a diamond anvil cell with a methanol-ethanol mixture (4:1) and with argon and helium as pressure-transmitting media, indicate stability of the cubic low-pressure modification below 5(1) GPa. In direction of increasing pressures, the onset of the transformation into a high-pressure phase (HP-Cu_3N) is observed around 5 GPa (Figure 3 and Figure 4). The evaluation of the diffraction patterns in direction of increasing pressure (Figure 3) indicates a two-phase region, in which residual LP-Cu_3N and the high-pressure phase coexist. The coexistence regime in experiments with alcohol mixtures as pressure medium is significantly smaller than with argon, which is attributed to a coupling of the stress-components to the phase transitions. The resulting overlap of unresolved reflections with diffraction angles of, e.g. 2θ = 10.8 and 12 degrees, obscure the lattice parameters and thus the volume determination. Consequently, no structure refinements were performed between 4.5 and 8.7 GPa. According to the data with argon as pressure medium the phase transition is reversible with a hysteresis of about 2 GPa. In accordance with this finding, ex-situ investigations in a multi-anvil press show re-formation of pure normal-pressure Cu_3N as revealed by X-ray powder diffraction patterns. Thus, the available experimental data are in agreement with the assumption that the composition of the high-pressure phase corresponds to that of the low-pressure modification within the limits of experimental error.

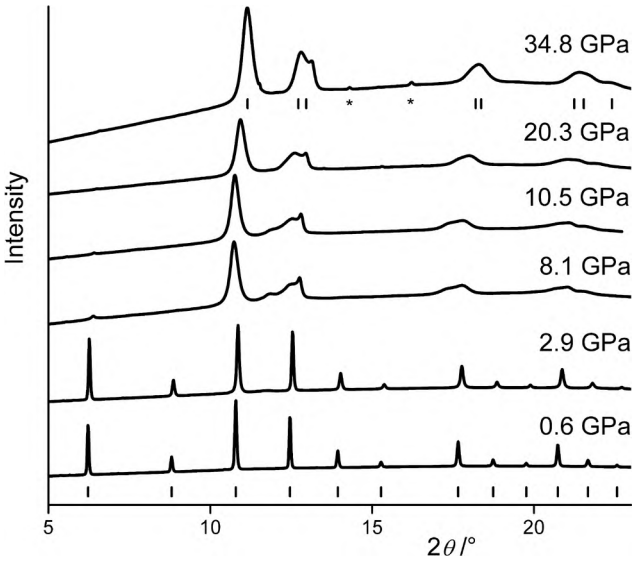

Figure 3. X-ray powder diffraction pattern (λ = 41.3082 pm) collected on increasing pressure with helium as pressure medium. The positions of the diffraction lines are marked on the bottom and top for LP-Cu_3N and HP-Cu_3N respectively. Stars mark the strongest reflections of the pressure medium.

The X-ray powder diffraction patterns at pressures above the structural phase transition differ significantly in runs with different pressure media (see Figure 5). Thus, the discussion of structure models is based on the diffraction data measured with helium as pressure transmitter in direction of increasing pressures only, since helium exhibits the smallest deviation from hydrostatic conditions. The intensity distribution of the HP-phase resembles roughly that of *fcc* copper, but splitting of the $(200)_{fcc}$ and $(220)_{fcc}$ reflections indicate a lower symmetry (see Figure 3). Choosing the tetragonal subgroup $I4/mmm$ ($a \approx$ 260 pm, $c \approx$ 380 pm) the most intense lines can be indexed satisfactory, especially at pressures exceeding 30 GPa. However, further peak splitting [especially of $(220)_{fcc}$] and addi-

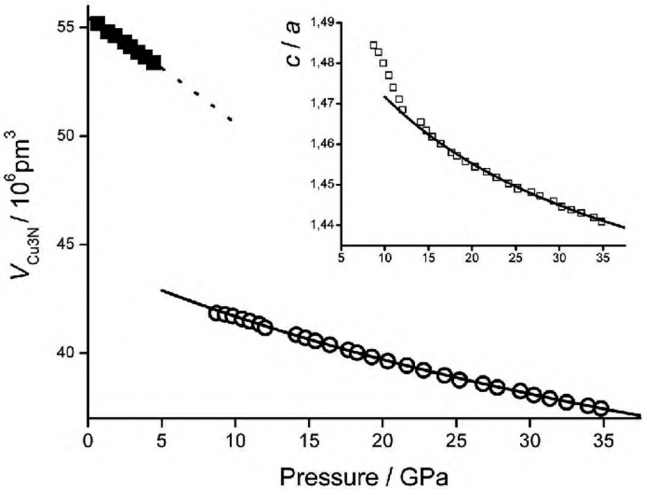

Figure 4. Change of the atomic volume of Cu_3N with increasing pressure (data with helium as pressure transmission medium only, for hysteresis see main text). The insert shows the change of *c*/*a* for the high-pressure phase. The line represents the quotient of the fitted equation of states for the lattice parameters.

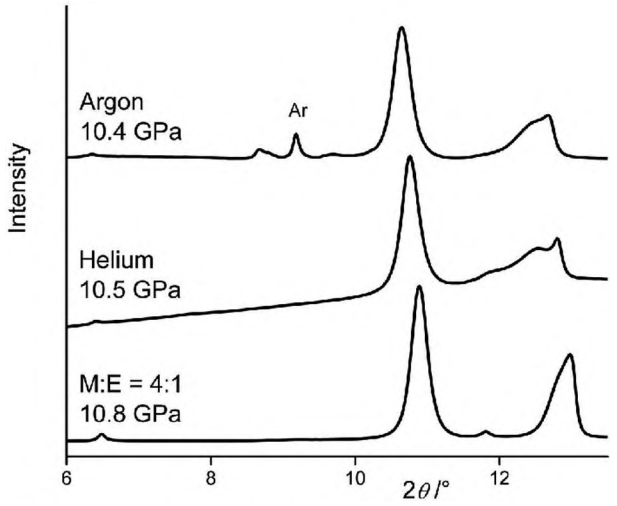

Figure 5. Comparison of X-ray powder diffraction data of HP-Cu_3N ($\lambda \approx 41$ pm) recorded in runs with different pressure media (methanol:ethanol = 4:1). The diagrams indicate intensity changes, which are attributed to different stress conditions and the resulting differences for the formation of HP-Cu_3N. Please note the superstructure reflections at approximately 6.4 ° and 11.8 °.

tional lines (at $2\theta \approx 6.4°$ and $2\theta \approx 11.8°$) evidence an even lower symmetry (or a hitherto unidentified second phase). Aiming to describe these additional lines, a model in orthorhombic space group *Immm* was chosen. Additionally, the observed peak broadening was described by a phenomenological model, which takes into account the effects of strain [8]. At 10.5 GPa, the refinements yield a small, but significant deviation from tetragonal symmetry with a = 380.2(2) pm, b = 393.5(2) pm, and c = 742.7(3) pm (see Figure 6). The atomic volume of the orthorhombic space group *Immm* indexing differs by only 0.1 % from the tetragonal solution, so that we take the higher symmetry data for the pressure-volume relation.

Intensity calculations indicate that the tetragonal partial structure of the high-pressure modification does not resemble any of the known modifications of the well-studied isotypic ReO_3 or any of the favorable structure types considered in the previous structure predictions from electronic structure calculations [4, 5]. According to the X-ray diffraction data, the copper substructure adopts a tetragonal body centered arrangement [copper atoms occupying position $2b$ $(0,0,^1/_2)$ of $I4/mmm$], which resembles the motif of the indium metal structure, but the nitrogen positions could not be reliably located by means of the X-ray diffraction experiments because of the disadvantageous ratio of the X-ray scattering factors (Table 1).

Aiming to locate the nitrogen atoms in the crystal structure, we performed high-pressure neutron diffraction experiments since copper and nitrogen have very similar neutron scattering factors [b(Cu) = 7.9 fm, b(N) = 9.4 fm]. The pressure-induced volume changes correspond to the data obtained from X-ray diffraction. Figure 7 shows neutron diffraction patterns at different pressures. Next to reflections arising from Cu_3N, reflections of lead (pressure marker), WC (anvil material), and nickel (crucible material) are visible. The phase transition of Cu_3N is clearly indicated by the disappearance of reflections

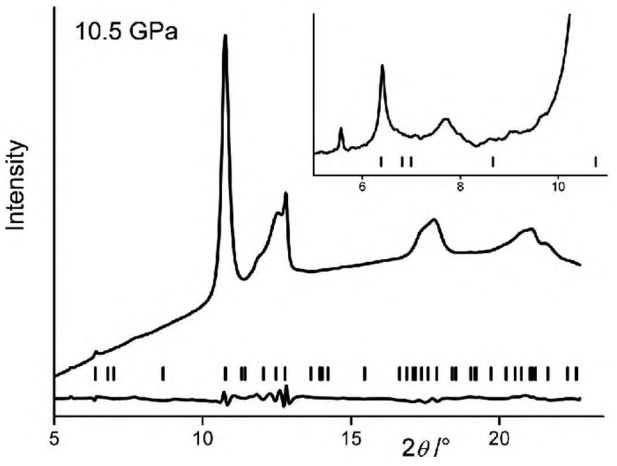

Figure 6. Diffraction pattern and difference between observed and calculated intensities of HP-Cu_3N in the orthorhombic space group *Immm* using a phenomenological strain model. The insert shows a magnification of the low angle part of the diffraction pattern including weak unindexed reflections.

of low-pressure copper nitride. The reflections due to high-pressure copper nitride only slowly grow from the background on increasing pressure and stay broad and weak. This fact is best seen from the reflections at TOF ≈ 18 μs: For LP-Cu_3N the (100) reflection presents as strongest signal. At 6.9 GPA no trace of this reflection is left in the pattern. Within the experimental resolution the tetragonal substructure can clearly be confirmed, but because of the experimental conditions given by the high-pressure set-up (signal to noise ratio limited by the small sample volume, additional scattering contributions of container material, anvil, and pressure marker) superstructure reflections are not detected in the neutron scattering data. The

Table 1. Crystallographic data of Cu_3N.

Low-pressure phase X-ray diffraction data [a), b)]	
Pressure /GPa	4.5
Space group	$Pm\bar{3}m$ (no. 221)
Lattice parameter /pm	376.52
Copper position	½, 0, 0
Nitrogen position	0, 0, 0
High-pressure phase X-ray diffraction data[a)]	
Pressure /GPa	8.7
Space group	*I*4/*mmm* (no. 139)
Lattice parameters *a* /pm	265.88
c /pm	394.69
Copper position	0, 0, 0
Neutron diffraction data[c)]	
Pressure /GPa	8.2
Space group	*I*4/*mmm* (no. 139)
Lattice parameters *a* /pm	265.5(1)
c /pm	391.1(3)
c/*a*	1.47
Copper position	0, 0, 0
Nitrogen position	½, ½, 0
Site occupancy factor of N	0.33(1)

a) Synchrotron data (ESRF, ID 09A, λ = 41.3082 pm).b) Ambient pressure: *a* = 381.48(9) pm. c) Time of flight data of the white spallation source at Rutherford Appleton Laboratory, Pearl diffractometer.

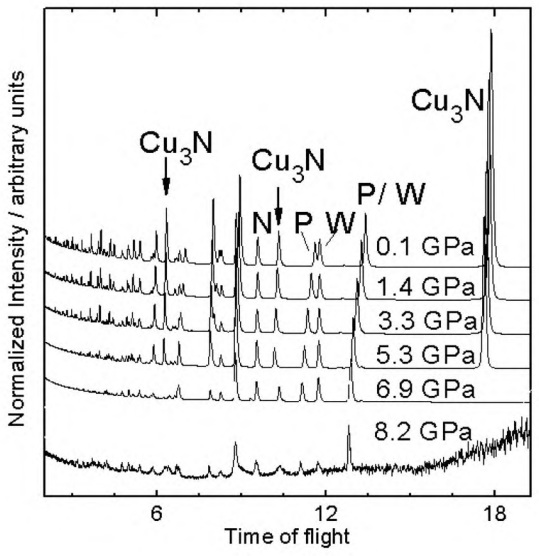

Figure 7. Neutron diffraction patterns (TOF in μs) of Cu_3N measured at different pressures. N, P, and W assign prominent reflections of nickel crucible, lead pressure indicator and WC anvils, respectively.

absence of extra reflections would indicate that under the pressure conditions of the neutron scattering experiment nitrogen atoms are randomly disordered in the overall crystal structure of the high-pressure phase. The structure refinement with nitrogen atoms disordered in the distorted octahedral voids of the tetragonal body-centered copper substructure leads to an occupation of 0.33(1) for the pattern at 8.2 GPa and by this in the description in space group *I*4/*mmm* (Table 1) to an unit cell content of $Cu_2N_{0.66(1)}$, which resembles the composition $Cu_3N_{1.0(1)}$. However, refinements of different patterns in the pressure range of about 8.2–9.5 GPa result in a site occupancy variation from 0.28–0.38, i.e., compositions in the range from $Cu_3N_{0.84}$ to $Cu_3N_{1.14}$.

Figure 8 shows the average tetragonal arrangement. Interatomic distances *d*(Cu–N) of $^4/_3 \times 187.6(1)$ pm and $^2/_3 \times 195.4(1)$ pm at 8.2 GPa are in agreement with the value observed for the ambient pressure ReO_3-type structure with *d*(Cu–N) = 191 pm [1, 2]. The complete structure model represents an elongated rocksalt structure with disordered defects in the anionic substructure. Thus, HP-Cu_3N fits well into the majority of well-studied and technologically relevant binary transition metal nitrides, in which nitrogen is located in octahedral voids. Moreover, a similar structure is known for the ambient temperature form of θ-Mn_6N_{5+x} realizing a tetragonal defect rocksalt structure. The reason for the distortion in the manganese case is believed to be the antiferromagnetic order [9]. Similarly, for CrN the cubic rocksalt type structure at ambient temperature distorts to orthorhombic below the Néel temperature because of magnetic ordering [10]. Still, the absence of magnetic moments in copper nitride leaves the reason for the distortion in the title compound unknown. Parallel performed electronic structure optimizations with the disordered structure model for the high-pressure phase of Cu_3N relax with the *c*/*a* ratio of a cubic *fcc* lattice. This disagreement to the experimental data can be taken as an indication for an ordered structural ground state, at least at the local level of several unit cell sized domains (see below).

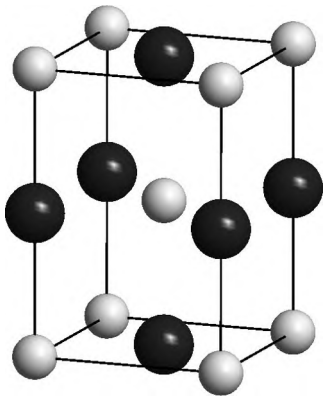

Figure 8. Average tetragonal crystal structure of the high-pressure modification of Cu_3N from experimental data. White spheres correspond to copper atoms. Nitrogen positions (dark spheres) are only occupied to $^1/_3^{rd}$.

A comparison of the unit cell volumes reveals that the structural transformation from the low-pressure into the high-pressure phase is associated with a discontinuous change of volume of about –20 %. However, consideration of a peculiar volume scatter in data with alcohol as pressure transmitting medium may allow for an alternative explanation involving a slight change of the chemical composition from Cu_3N to a

nitrogen-richer phase. The subsequent production of elemental copper might not be detectable in the products after pressure release with diffraction techniques and additionally be shaded by the occasional copper formation because of decomposition of the metastable LP-Cu_3N triggered by shear-forces. This and further open points are going to be addressed by electronic structure calculations.

The magnitude of the volume change associated with the phase transformation can be compared to an estimation based on an analysis of sphere packing. In the ambient-pressure phase of Cu_3N with linearly coordinated copper, the metal atoms adopt a defect variant of an *fcc* arrangement, in which only 75 % of the atomic positions are filled. The high-pressure modification adopting a body centered tetragonal copper arrangement can be described as a slightly distorted *fcc* pattern of metal atoms, in which all positions are occupied. As a result, the packing density of the metal atoms is significantly increased and accounts surprisingly well for the experimentally observed volume change of –20 %.

A compressibility of B_0 = 114(2) GPa for LP-Cu_3N results from application of a least-squares refinement of a linear equation to the experimental data (V_0 = 55.48(2) × 10^6 pm^3). This bulk modulus is surprisingly similar to the value for the isotypic ReO_3 phase (100 GPa [11]) and to a value obtained from electronic structure calculations (115.2 GPa) [12]. An increased resistance of the linear arrangement at Cu^I against bending deformation is indicated by the different structural high-pressure behavior of Cu_3N and isostructural ReO_3, explaining the absence of distortion variants because of octahedra rotation for the nitride. The linear thermal expansion of LP-Cu_3N below ambient temperatures is in the normal range for semiconductors, and also indirectly supports this view. For comparison, the linear thermal expansion of ReO_3 has a small positive or even negative value depending on temperature because of intensifying thermal rotation of the $ReO_{6/2}$ octahedra, i.e., smaller angles at the bridging oxygen atoms with increasing temperatures [13].

Concomitant with the discontinuous volume alteration, dramatic changes occur in the electronic properties, as indicated by the pressure-dependent optical response. The pressure-dependent transmission and absorption spectra in the infrared and visible frequency range are depicted in Figure 9. At the lowest applied pressure (1.0 GPa), we observe a strong increase of the absorption (indicated by an arrow) at around 8000 cm^{-1} (1 eV) because of excitations across the bandgap. The location of the absorption edge is in good agreement with the calculated bandgap earlier estimated from electronic structure calculations (0.9 eV) [14]. For pressures above ≈ 4 GPa, the absorption strongly increases in the infrared frequency range, which can be attributed to additional electronic states close to the Fermi level induced by pressure. Above ≈ 7 GPa, the changes with increasing pressure are small and the absorption spectrum is almost flat. These findings suggest that Cu_3N undergoes a transition from a semiconductor to a metal induced in the pressure range 4–7 GPa. A similar pressure range for the pressure-induced semiconductor–metal transition was earlier observed in electrical resistivity measurements in diamond anvil cells [6, 7]. Upon pressure release, the initial low absorption level in the infrared range is not recovered, as illustrated by the spectrum for 1.8 GPa (see Figure 9b); this finding is in agreement with the hysteresis observed in our pressure-dependent diffraction measurements and with the pressure-dependent electrical resistivity measurements [7].

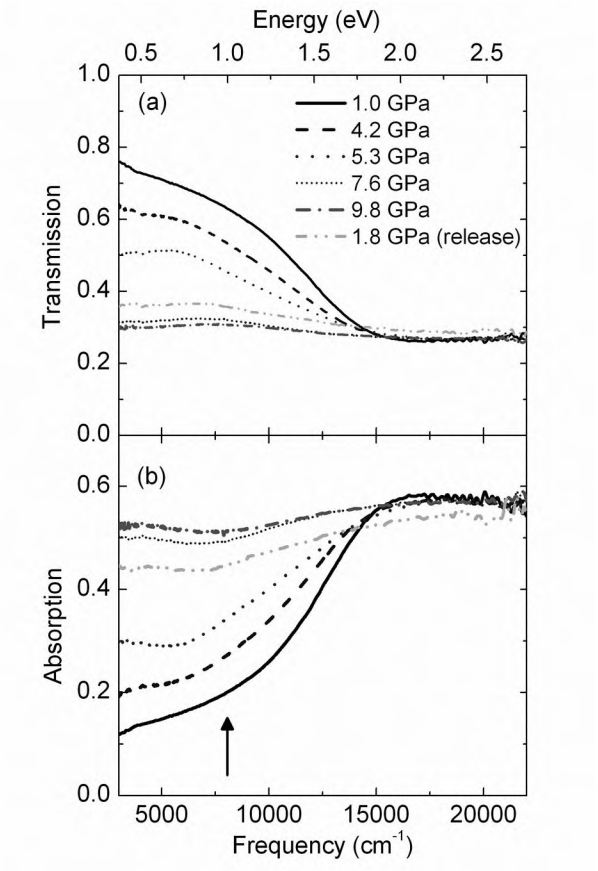

Figure 9. (a) Transmission $T(\omega) = I_s(\omega)/I_r(\omega)$ (see text for definitions) of Cu_3N at ambient temperature as a function of pressure and (b) the corresponding absorption $A = \log_{10}(1/T)$ as a function of pressure. The arrow in (b) indicates the frequency position of the absorption edge.

As a first step in electronic structure calculations, and a quality assurance for the selected method, we reproduced the experimentally obtained properties for ReO_3 type LP-Cu_3N. For this purpose, the optimized arrangement and total energy was calculated by fully relaxing the structure. The obtained lattice parameter of the LP-Cu_3N (Table 2) fits well with the experimental data. It is slightly overestimated (0.8 %) by the calculation, a typical peculiarity of the generalized gradient approximation (GGA). A comparison with the total energy of the elements (3 Cu + $^1/_2$ N_2) demonstrates the known metastability of LP-Cu_3N. The calculated heat of formation at 0 Kelvin yields to ΔH_f = 1.21 eV per formula unit. Subsequently, we developed the energy–volume curve (Figure 10, left) by fitting the 15 $E(V)$ data points with the Murnaghan equation of state.

Next, total energy calculations of the experimentally suggested structure with the composition Cu_3N were performed. Because of the proposed disordered nitrogen atoms, a supercell

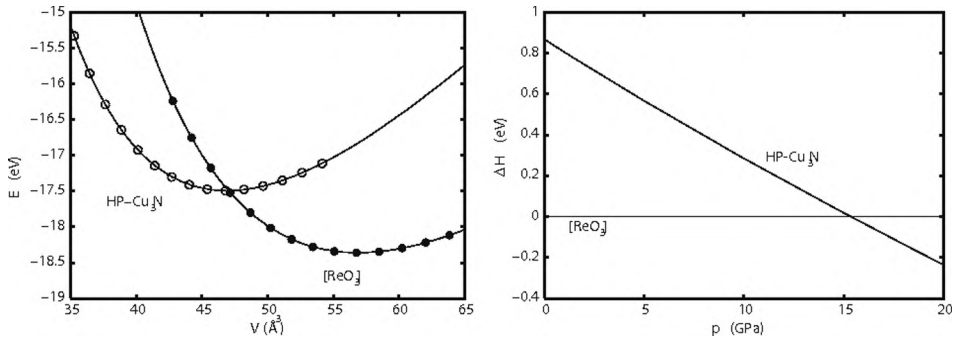

Figure 10. Energy–volume- (left) and enthalpy–pressure-diagram (right) of the ReO_3 type LP-Cu_3N and the proposed high-pressure phase.

technique was employed (3 × 3 × 3 unit cells containing 54 copper atoms and 18 nitrogen atoms). Twenty different cells were created by randomly occupying 18 of the 54 octahedral voids with nitrogen. All structures have been automatically relaxed under the constraint of fixed atom positions (else the structure would break down, because supercells are, unfortunately, far away from a statistically occupied crystal). The variation in total energy within the 20 structures is only 1.7 %, in volume it is less than 1 %. Because of these results, we reason that the supercell is large enough to approximately represent the entire crystal. The average lattice parameters for the conventional unit cell at zero pressure are a = 2.81 Å and c = 3.95 Å. The phase transition enthalpy from the ReO_3-type to the most stable nitrogen distribution amounts to 0.87 eV per formula unit, the volume of the potential high-pressure phase is about 18 % smaller. This volume decrease in combination with the not too large endothermic enthalpy indicates a possible high-pressure transition. Namely, for the approximation of same bulk moduli one can calculate a zeroth order transition pressure of $p_{trans} = -\Delta E/\Delta V \approx 11$ GPa. Hence, and to make a comparison with the experimental results possible (that are only available at high pressures); we investigated the compounds' properties under pressure as described above and obtained the E–V and the ΔH–p curves. Both are displayed in Figure 10. Some further physical properties of the LP-Cu_3N and the proposed high-pressure phase are listed in Table 2. The energy–volume diagram shows the smaller equilibrium volume and higher energy of the high-pressure phase. As a consequence, at pressures above 16 GPa it becomes thermodynamically stable, as the enthalpy–pressure diagram evidences. At the experimentally detected transition pressure, the compound is 0.39 eV less stable than LP-Cu_3N (Table 2), its volume is about 7 % larger than the experimentally obtained one. However, most profound is the deviation of the c/a ratio. All 20 statistically occupied structures relax from the experimentally start value of c/a = 1.50 to one between 1.37 and 1.43 in the course of calculation. Even at high pressures this ratio remains. Conspicuously, the average ratio has been calculated to 1.41 ≈ $\sqrt{2}$. A body centered tetragonal cell with $c/a = \sqrt{2}$ means nothing else but a face centered cubic (*fcc*) cell. With the aim to audit this result and exclude errors because of too small supercells, we repeated the calculation with a larger 5 × 5 × 3 supercell containing 150 copper and 50 nitrogen atoms. The c/a ratio decreased again from the start value 1.50 to 1.417 and confirmed our previous result. The thought that *fcc* copper incorporates nitrogen statistically onto the octahedral voids and remains *fcc*, is not farfetched. As was already commented in the discussion of the experimental results, the reason for the tetragonal distortion is unknown. From the theoretical point of view, the reason does not exist and the structure relaxes into the more stable cubic one. Nonetheless, the statistical occupied *fcc* type Cu_3N is more stable than all other yet considered alternatives.

The finding of elemental copper produced in few pressure experiments, leads to the speculation about a slight change in chemical composition. Possibly, this different composition is responsible for the tetragonal distortion. We took this into account by creating each ten of 3 × 3 × 3 supercells with the compositions $Cu_{54}N_{19}$, $Cu_{54}N_{20}$, and $Cu_{54}N_{21}$ and an initial c/a value of 1.50. All compounds were relaxed with respect to the volume and the cell geometry. The results for the c/a ratio and the theoretical reaction enthalpies for

$$(1 + x)\ \text{LP-Cu}_3\text{N} = \text{HP-Cu}_3\text{N}_{1+x} + 3x\ \text{Cu}$$

Table 2. Comparison between experimentally and theoretically obtained properties of LP-Cu_3N and the proposed tetragonal high-pressure structure.

		ReO_3 type		HP-Cu_3N		
Lattice constants	Experiment (0 GPa)	p = 0 GPa	p = 8.2 GPa	p = 0 GPa	p = 8.2 GPa	Experiment (8.7/8.2 GPa)
a /Å	3.807(4) [1]	3.84	3.77	2.81	2.76	2.6588/2.655(1)
c /Å	–	–	–	3.95	3.87	3.9469/3.911(3)
c/a	–	–	–	1.41	1.40	1.50/1.47
V /Å^3/f.u.	55.18	56.6	53.5	46.9	44.5	41.89/41.34
ΔH /eV/f.u.	–	0	2.82	0.87	3.21	–

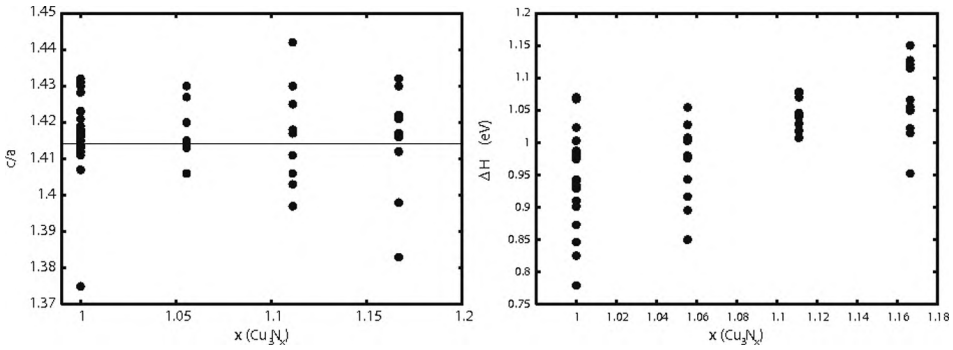

Figure 11. Tetragonal lattice parameter ratio c/a (left) and associated heat of formation (relative to low pressure Cu_3N) per formula unit in dependence of the nitrogen content (right).

are shown in Figure 11. The nitrogen content seems to have no influence on the c/a ratio. The values for all compositions relax downwards and are finally distributed around $\sqrt{2}$ again. Also, the reaction enthalpies give no hint that a disproportionation into elemental copper and a nitrogen richer phase is lucrative.

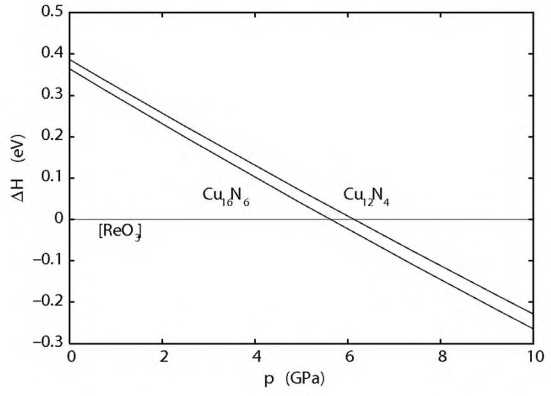

Figure 12. ΔH–p diagram of the nitrogen ordered phases $Cu_{12}N_4$ and $Cu_{16}N_6$ relatively to the low pressure ReO_3-type.

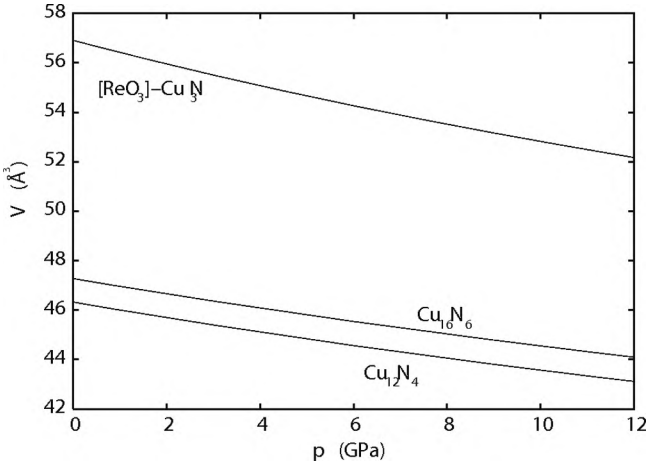

Figure 13. V–p diagram of the nitrogen ordered phases $Cu_{12}N_4$, $Cu_{16}N_6$ and the low pressure Cu_3N.

With the purpose to simulate the actual experimentally identified structure, i.e. a relaxed groundstate, whose properties fit with the experimental ones, we allowed a more regular arrangement of the nitrogen atoms. A representative compound AB_3, that crystallizes in a *bct* sublattice of *B* and the octahedral voids filled with *A* atoms, does, to the best of our knowledge, not exist. Hence, we occupied 2 × 2 × 2 (16 copper atoms) and 3 × 3 × 3 (54 copper atoms) copper *bct* sublattices with 6 respectively 18 nitrogen atoms in a way that the compound will presumably retain its dilation in *c* direction. The latter supercell represents the suggested composition Cu_3N, whereas the smaller supercell has a nitrogen content of 0.375 ($Cu_3N_{1.125}$). We found just a few unit cells that satisfied the requirements of both a tetragonal symmetry and the approximated experimentally detected ratio of the lattice parameters (Figure 12 and Figure 13). The data of the most promising structure for each composition are shown in Table 3, the unit cells are presented in Figure 14. The formulas document the resulting size of the unit cell (caused by symmetry reduction in the case of $Cu_{12}N_4$). In order to avoid confusion between the statistical and ordered structures we retain this labeling for the following. As one can read from Table 3, both the $Cu_{16}N_6$ and the $Cu_{12}N_4$ remain tetragonal during the relaxation with an optimized c/a ratio of 1.51 respectively 1.49. At zero pressure, a transition from the low-pressure ReO_3 type under conservation of the composition would require 0.39 eV, a disproportionation into copper and $Cu_{16}N_6$ 0.36 eV. That means, that this ordered tetragonal compounds are about 0.5 eV per formula unit Cu_3N more stable than the most stable calculated statistical and hence cubic structure. The subsequent high-pressure examination produced results that are shown in Figure 14. Some more detailed properties at the experimentally described pressure of 8.2 GPa are shown in Table 3 for comparison. Both ordered phases become more stable with respect to the LP-Cu_3N at about 6 GPa, the nitrogen-richer phase is a little bit more stable over the total pressure range. However, the enthalpy difference is at each pressure just 0.03–0.04 eV, too little for a substantiated interpretation. The c/a ratio of $Cu_{16}N_6$ amounts 1.50 at pressures around 8 GPa and agrees with the experimentally found value in X-ray diffraction at 7.8 GPa, for

$Cu_{12}N_4$ it decreases under pressure and agrees at ca. 8 GPa with the experimental data from neutron diffraction at 8.2 GPa. The volume decrease caused by the phase change has been measured to be approximately 20 %, for $Cu_{12}N_4$/$Cu_{16}N_6$ it amounts to about 18 % and 16 %, respectively. The corresponding lattice parameters are 2 % overestimated, in good accordance with the expected overestimation because of the GGA approximation. However, considering both unit cells, one finds a chemical counterintuitive situation. For the composition $Cu_{16}N_6$, the most likely coordination for the metal would be square-planar for two Cu^{2+} and linear for 14 Cu^{+}. But we find also T-shaped coordination as well as nitrogen-uncoordinated copper. For $Cu_{12}N_4$, a regular linear coordination of the copper atoms would be intuitive, but this structure suggestion has beside this coordination numbers of 0, 1, and 3. This situation is implausible; albeit it is to consider that the proposed statistical occupation will offer all kinds of these coordination environments, too. In the sum, because of tremendous possibilities to distribute the nitrogen atoms in an ordered way and furthermore the unusual coordination of copper in this two suggestions, we don't want to claim that one of these is the true structure of high-pressure Cu_3N. At this point, let us recall the above depicted irregularities detected in some experiments. One possibility that would explain all of these facts is the formation of different phases (potentially because of small local pressure variation) side by side. It was already mentioned that a production of copper metal can be attributed to pressure gradients and shear stresses. The very small enthalpy differences between the different ordered phases support this idea. Additionally, this would explain that an ordering of nitrogen cannot be found in the diffraction data. But these considerations should just be taken as a careful guess to bring together the experimental and theoretical results. However, all theoretical findings in this work indicate that a kind of nitrogen ordering exists in HP-Cu_3N. For a final clarification further work is required.

Table 3. Calculated unit cell data and heat of formation with reference to LP-Cu_3N for the most promising ordered compounds Cu_3N and $Cu_3N_{1.125}$.

Compound	Space group	a /Å	c /Å	c/a	V /Å^3	ΔH /eV
			p = 0 GPa			
$Cu_{16}N_6$	$P4_2/mmc$ (131)	3.89	16.60	1.51	47.2	0.36
$Cu_{12}N_4$	$P\bar{4}m2$ (115)	3.88	12.27	1.49	46.2	0.39
			p = 8.2 GPa			
$Cu_{16}N_6$	$P4_2/mmc$ (131)	3.71	4.07	1.50	45.0	–0.16
$Cu_{12}N_4$	$P\bar{4}m2$ (115)	3.71	3.99	1.47	44.0	–0.12

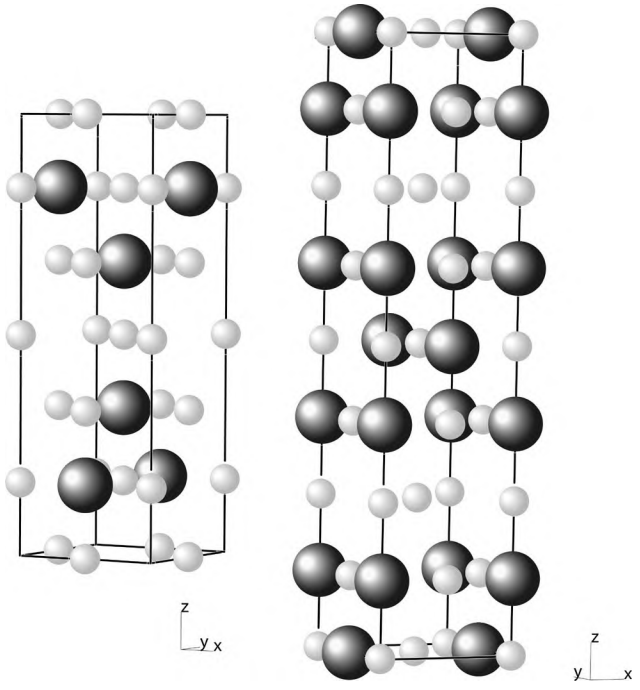

Figure 14. Unit cells of the nitrogen-ordered structure suggestions $Cu_{12}N_4$ (left) and $Cu_{16}N_6$ (right). N = dark spheres, Cu = light spheres.

Conclusions

With the conversion from the open framework inverse ReO_3 crystal structure to a copper substructure of one of the dense sphere packings we find a transition from a semiconductor dominated by covalent Cu–N bonding to an interstitial metallic nitride. Thus, the high-pressure phase of Cu_3N connects to the binary nitride phases known from the neighboring 3d elements both in crystal structure and physical properties.

Our total energy calculations and high-pressure investigations support the experimental findings. Independent of the nitrogen distribution on the octahedral voids of the copper sublattice, this type is more stable than the former theoretically discussed promising structure types. However, for disordered nitrogen atoms, the structure relaxes into an *fcc* structure. Even disordered phases with higher nitrogen contents prefer this pattern. A reason for the tetragonal distortion cannot be found. For a total agreement with the experimentally detected transition pressure and lattice parameters, there is a need for an ordering of the nitrogen atoms. We offer suggestions for possible structures of HP-Cu_3N, that fulfill all required properties, but the coordination polyhedra in these phases are chemically counterintuitive. A slight nitrogen enrichment that has been considered because of experimentally detected elemental copper is likewise advantageous and cannot be fully excluded. To our opinion, the structure of the copper sublattice in HP-Cu_3N is enlightened, but the distribution of the nitrogen remains an open question.

Experimental Section

Preparation and Characterization

Microcrystalline LP-Cu_3N was prepared from CuF_2 in flowing ammonia at 270 °C for 5 h. Higher temperatures or longer reaction times led to the formation of increasing amounts of elemental copper, which indicated that Cu_3N is metastable at the synthesis conditions.

X-ray powder diffraction was carried out with an Imaging Plate Guinier Camera (HUBER diffraction, Cu-$K_{\alpha1}$ and Co-$K_{\alpha1}$ radiation,

6 × 15 min scans, 8 ° ≤ 2Θ ≤ 100 °). Refinements of the cubic lattice parameter by a least-squares procedure resulted in a = 381.48(9) pm compared to 381.7(1) pm obtained with single crystals [2] and 380.7(4) pm from microcrystalline powders [1]. Patterns between ambient temperature and 20 K were recorded in the range of 15 ° ≤ 2Θ ≤ 90 ° (Cu-$K_{\alpha 1}$) to analyze the thermal expansion of LP-Cu_3N. No low-temperature phase transition was observed; the linear expansion coefficient for the investigated temperature range resulted in α = 6.4(3) × 10^{-6} K^{-1}.

Chemical analyses on O and N were performed using the carrier gas hot-extraction technique on a LECO analyzer TCH-600. All values are averages of at least three independent measurements. Chemical analysis of the starting material resulted a composition of $Cu_3N_{0.980(7)}O_{0.05(2)}$ [w(O) = 0.40 ± 0.14 %, w(N) = 6.68 ± 0.05 %].

DTA/TG-measurements were performed with a STA 449C analyzer (flowing oxygen, argon, or nitrogen atmosphere, 99.999 %, thermocouple type S, NETZSCH Gerätebau, Selb). Temperature calibration was obtained using five melting standards in the temperature range of 370 K ≤ T ≤ 770 K. In pure oxygen atmosphere Cu_3N slowly gains weight above 473 K. At a heating rate of 10 K·min^{-1}, the exothermic oxidation was accelerated at higher temperatures and was completed at about 650 K with an overall weight gain of 16.1 % forming pure CuO (calcd.: +16.6 %). In argon or nitrogen atmosphere, an exothermic reaction starting at about 700 K indicated the metastable nature of low-pressure Cu_3N. In accordance with the observed weight loss of –7.0 %, the decomposition reaction produced pure copper as exclusive solid product (calculated mass difference –6.8 %).

Ex-situ High-pressure Synthesis Experiments and Characterization

High-pressure conditions were realized with a hydraulic uniaxial press. Force redistribution in order to achieve quasi-hydrostatic conditions was accomplished with a Walker-type module (two-stage assembly with a central octahedral pressure chamber) and MgO/Cr_2O_3 octahedra with an edge length of 14 mm or 18 mm. Elevated temperatures were realized by resistive heating of graphite tubes containing the sample crucible. Pressure and temperature calibration was completed before the experiments by analyzing the resistance changes of bismuth and lead [15] and measuring set-ups equipped with a thermocouple, respectively. The crucibles girdling the sample mixtures were made from hexagonal boron nitride. X-ray powder diffraction data and energy dispersive X-ray analysis did not give evidence for a reaction of the container with the sample. Thus, separation of reaction products and crucible material could be achieved easily. A typical high-pressure synthesis required pressure increase for 3 h, holding at the maximal pressure for typically 5 h followed by pressure decrease in 10 h. During maximum pressure of 9(1) GPa same samples were heated at 500(70) K for 10 min. Heated samples were quenched to ambient temperature by disconnecting the heating current before decompression.

In-situ Diffraction Experiments at High Pressures

Copper nitride was ground into a fine powder and placed in steel gaskets by using a 4:1 methanol/ethanol mixture, argon, or helium, respectively, as pressure transmitting medium. High pressures were generated by diamond anvil cells and determined by the ruby luminescence method. X-ray powder diffraction experiments were carried out at the undulator beamline ID 9A of the ESRF, Grenoble. During the exposures samples were oscillated by ±3 ° in order to enhance powder statistics. Typical exposure times were two to five seconds. The diffraction patterns were collected on an imaging plates detector, which is positioned at a distance of approximately 450 mm from the sample. For calibration of wavelength and detector distance we used a silicon standard sample. Integration of the two-dimensional raw data was performed by using the pattern integration software image integrator [16]. Peak positions and lattice parameters were refined using the computer program WinCSD [17].

Neutron diffraction under hydrostatic pressures was performed at the High Pressure Facility at the Pearl beamline of the ISIS pulsed-neutron source at the Rutherford Appleton Laboratory as time-of-flight experiment. High pressure was obtained in a nickel crucible using a Paris-Edinburgh cell equipped with standard tungsten carbide anvils. Here, a small lead sphere was used as a pressure sensor and quasi-hydrostatic pressure conditions were realized with methanol as pressure transmitting medium. Earlier diffraction experiments in diamond anvil cells (see above) indicated stability of Cu_3N in alcohol (4:1 mixture of methanol and ethanol) up to 30 GPa. Structure refinements were performed with the program system GSAS [18] within the graphical interface EXPGUI [19].

In-situ Optical Spectroscopy

Pressure-dependent absorption measurements were performed in the infrared and visible frequency range with a Bruker IFS 66v/s spectrometer with an infrared microscope (Bruker IRscopeII). The measurements were partly carried out at the infrared beamline of the synchrotron radiation source ANKA (Angströmquelle Karlsruhe). A diamond anvil cell was used for generation of pressures up to 10 GPa and the ruby luminescence method was used for pressure determination. As hydrostatic pressure transmitting medium we used argon. In order to determine the transmission of Cu_3N under pressure, the intensity $I_s(\omega)$ of the radiation transmitted by a small amount of the powder sample and the pressure transmitting medium was measured. As reference, the intensity $I_r(\omega)$ transmitted by the empty diamond anvil cell was used. The transmission was then calculated according to $T(\omega) = I_s(\omega)/I_r(\omega)$. The absorption was calculated as $A = \log_{10}(1/T)$.

Electronic Structure Calculations

The first-principles electronic-structure calculations of density-functional type were performed by using the Vienna ab initio simulation package [20, 21], plane-wave basis sets and ultra-soft pseudopotentials. The exchange-correlation energy was treated in the generalized gradient approximation (GGA) [22]. The plane-wave cutoff energies were chosen to be 500 eV. The Brillouin zone integrations were performed using the scheme of *Monkhorst* and *Pack* [23]. Optimized structural models were obtained by relaxing all forces to values below 10^{-3} eV·$Å^{-1}$ and stresses below 1 kbar. To examine the structural behavior at high-pressures, all total energies E were re-calculated under compression and expansion, and the lattice parameters were scaled in steps of 1 % from 91–105 % of the minimum geometries. The 15 E – V data points can be fitted by the Murnaghan equation of state [24]. From these the enthalpy–pressure curve easily can be deduced by calculating $p = -\delta E/\delta V$ and $H = E + pV$.

Acknowledgement

We thank *Dr. Raúl Cardoso* for the collection of the ambient pressure X-ray powder diffraction data, *Susann Leipe* and *Dr. Peter Höhn* for

experimental support, *Anja Völzke* for performing the chemical analyses, *Susann Müller* for the operating of the thermal analysis, and *Prof. Yuri Grin* for valuable discussions. Additionally we wish to acknowledge the assignment of beamtime at the ISIS pearl high-pressure facility and at the undulator beamline ID 9A of the ESRF. We acknowledge the ANKA Angströmquelle Karlsruhe for the provision of beamtime and we would like to thank *D. Moss, Y.-L. Mathis, B. Gasharova*, and *M. Süpfle* for assistance using beamline ANKA-IR. This work was supported by the *Max-Planck-Gesellschaft* and within the Schwerpunktprogramm "Synthesis, in situ characterisation, and quantum mechanical modelling of Earth Materials, oxides, carbides, and nitrides at extremely high pressures and temperatures" of the *Deutsche Forschungsgemeinschaft* (SPP 1236). Financial support through the *Emmy-Noether-Program* and the SFB 484 is gratefully acknowledged.

References

[1] R. Juza, H. Hahn, *Z. Anorg. Allg. Chem.* **1938**, *239*, 282–287.
[2] U. Zachwieja, H. Jacobs, *J. Less-Common Met.* **1990**, *161*, 175–184.
[3] J. E. Jorgensen, W. G. Marshall, R. I. Smith, J. S. Olsen, L. Gerward, *J. Appl. Crystallogr.* **2004**, *37*, 857–861 and references cited therein.
[4] Z. Cancarevic, J. C. Schön, M. Jansen, *Z. Anorg. Allg. Chem.* **2005**, *631*, 1167–1171.
[5] W. Yu, L. Li, C. Jin, *J. Mater. Sci.* **2005**, *40*, 4661–4664.
[6] L. X. Yang, J. G. Zhao, Y. Yu, F. Y. Li, R. C. Yu, C. Q. Jin, *Chin. Phys. Lett.* **2006**, *23*, 426–427.
[7] J. G. Zhao, L. X. Yang, Y. Yu, S. J. You, J. Liu, C. Q. Jin, *Phys. Status Solidi* **2006**, *243*, 573–578.
[8] a) P. W. Stephens, *J. Appl. Crystallogr.* **1999**, *32*, 281–289 b) R. E. Dinnebier, R. von Dreele, P. W. Stephens, S. Jelonek, J. Sieler, *J. Appl. Crystallogr.* **1999**, *32*, 761–769
[9] A. Leineweber, R. Niewa, H. Jacobs, W. Kockelmann, *J. Mater. Chem.* **2000**, *10*, 2827–2834.
[10] L. M. Corliss, N. Elliott, J. M. Hastings, *Phys. Rev.* **1960**, *117*, 929–935.
[11] J.-E. Jørgensen, J. Staun Olsen, L. Gerward, *J. Appl. Crystallogr.* **2000**, *33*, 279–284.
[12] Ma. Guadalupe Moreno-Armenta, W. López Pérez, N. Takeuchi, *Solid State Sci.* **2007**, *9*, 166–172.
[13] N. Matsuno, M. Yoshimi, S. Ohtake, T. Akahane, N. Tsuda, *J. Phys. Soc. Jpn.* **1978**, *45*, 1542–1544.
[14] U. Hahn, W. Weber, *Phys. Rev. B* **1996**, *53*, 12684–12693.
[15] D. A. Young, *Phase diagram of the elements*,University of California Press, Berkeley 1991.
[16] L. Akselrud, *Image Integrator*, Version 1.2, Max-Planck-Institut für Chemische Physik fester Stoffe, Dresden, **2005**.
[17] L. G. Akselrud, P. Y. Zavalii, Yu. N. Grin, V. K. Pecharsky, B. Baumgartner, E. Woelfel, *Mater. Sci. Forum* **1993**, *133–136*, 335–340.
[18] A. C. Larson, R. B. Von Dreele, *General Structure Analysis System (GSAS)*, Los Alamos National Laboratory Report **2004**, 86–748.
[19] B. H. Toby, *J. Appl. Crystallogr.* **2001**, *34*, 210–213.
[20] G. Kresse, J. Hafner, *Phys. Rev. B* **1993**, *47*, 558–561;G. Kresse, J. Hafner, *Phys. Rev. B* **1994**, *49*, 14251–14269.
[21] G. Kresse, J. Furthmüller, *Comput. Mater. Sci.* **1996**, *6*, 15–50;G. Kresse, J. Furthmüller, *Phys. Rev. B* **1996**, *55*, 11169–11186.
[22] J. P. Perdew in: *Electronic Structure of Solids '91* (Eds.: P. Ziesche H. Eschrig), Akademie Verlag, Berlin, **1991**, page 11.
[23] H. J. Monkhorst, J. D. Pack, *Phys. Rev. B* **1976**, *13*, 5188–5192.
[24] F. D. Murnaghan, *Proc. Natl. Acad. Sci. USA* **1944**, *30*, 244–247.